Available online at www.sciencedirect.com
ScienceDirect
Spectrochimica Acta Part A 70 (2008) 217–233
SPECTROCHIMICA ACTA PART A
www.elsevier.com/locate/saa

FTIR, magnetic, ^{1}H NMR spectral and thermal studies of some chelates of caproic acid: Inhibitory effect on different kinds of bacteria

Moamen S. Refat [a,*], Sabry A. El-Korashy [b], Deo Nandan Kumar [c], Ahmed S. Ahmed [a]

[a] Department of Chemistry, Faculty of Education, Port Said, Suez Canal University, Mohamed Ali Street, Port Said, Egypt
[b] Department of Chemistry, Faculty of Science, Ismalia, Suez Canal University, Ismalia, Egypt
[c] Department of Chemistry, Deshbandhu College, University of Delhi, New Delhi 110019, India

Received 10 May 2007; received in revised form 24 June 2007; accepted 3 July 2007

Abstract

A convenient method for the preparation of complexes of the Cr^{3+}, Mn^{2+}, Fe^{3+}, Co^{2+}, Ni^{2+}, Zn^{2+}, ZrO^{2+}, $UO_2{}^{2+}$, Zr^{4+} and Th^{4+} ions with caproic acid (Hcap) is reported and this has enabled 10 complexes of caproate anion to be formulated: $[Cr(cap)_3]\cdot 5H_2O$, $[Mn(cap)_2(H_2O)_2]$, $[Fe(cap)_3]\cdot 12H_2O$, $[Co(cap)_2(H_2O)_2]\cdot 4H_2O$, $[Ni(cap)_2(H_2O)_2]\cdot 3H_2O$, $[Zn(cap)_2]$, $[ZrO(cap)_2]\cdot 3H_2O$, $[UO_2(cap)(NO_3)]$, $[Zr(cap)_2(Cl)_2]$ and $[Th(cap)_4]$. These new complexes were synthesized and characterized by elemental analysis, molar conductivity, magnetic measurements, spectral methods (mid infrared, ^{1}H NMR and UV–vis spectra) and simultaneous thermal analysis (TG and DTG) techniques. It has been found from the elemental analysis as well as thermal studies that the caproate ligand behaves as bidentate ligand and forming chelates with 1:1 (metal:ligand) stoichiometry for $UO_2{}^{2+}$, 1:2 for (Mn^{2+}, Co^{2+}, Ni^{2+}, Zn^{2+}, ZrO^{2+} and Zr^{4+}), 1:3 stoichiometry for (Cr^{3+} and Fe^{3+}) and 1:4 for Th^{4+} caproate complexes, respectively, as bidentate chelating. The molar conductance measurements proved that the caproate complexes are non-electrolytes. The kinetic thermodynamic parameters such as: E^*, ΔH^*, ΔS^* and ΔG^* are estimated from the DTG curves. The antibacterial activity of the caproic acid and their complexes was evaluated against some gram positive/negative bacteria.

Keywords: Caproic acid; Infrared spectra; Thermodynamic paramenters; ^{1}H NMR spectra; Antibacterial activity

1. Introduction

The carboxylic acid complexes are very interesting [1] because they can contain two or more anti-ferromagnetically coupled metal centers [2–9]. Since each carboxylate oxygen atom has two lone pairs, they can either have only one lone pair involved in the coordination resulting in a dinuclear paddle-wheel structure or has the second lone pair donated to a metal ion of another paddle-wheel structure resulting in a polymeric structure. Also the binding of metal ions to carboxylic acids has been a subject of intense research with diverse applications, including as model systems for metalloactive sites in bioinorganic chemistry [10,11]. The structural diversity encountered in metal–carboxylate complexes can be attributed to the versatile bonding of the carboxylate group which can act as a bidentate ligand or a bridging ligand [1,12].

n-Caproic acid (*n*-hexanoic acid) (Scheme 1) $C_6H_{12}O_2$, occurs in milk fats (about 2%), and in coconut oil (<1%) and is employed in the manufacture of pharmaceuticals, esters for artificial flavors and of hexyl derivatives especially hexylphenols, hexylresorcinol [13]. It is slightly soluble in water and readily soluble in ethanol and ether [14].

Caproic acid has been used as a good extracting agent [15–17] for rare earths, zirconium, chromium, manganese, iron, gallium as well as aluminum with catechol violet by a mixture containing $CHCl_3$, caproic and propionic acids. Pietsch [18] extracted caproates of thorium, lead and iron into $CHCl_3$. Compounds of transition and non-transition elements with caproic acid are not so common. A literature survey reveals that there are some papers on the preparation of caproates of rare earth elements [19,20] and anhydrous copper(II) hexanoate from cuprous and cupric oxides [21]. Also, Refat et al. [22] have synthesized and characterized Cu(II), Cd(II), Pb(II) and Al(III) caproate complexes.

The present investigation was undertaken to study the course of the reaction of caproic acid with Cr(III), Mn(II), Fe(III),

* Corresponding author.
E-mail address: msrefat@yahoo.com (M.S. Refat).

1386-1425/$ – see front matter © 2007 Elsevier B.V. All rights reserved.
doi:10.1016/j.saa.2007.07.036

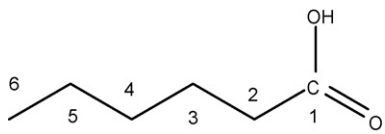

Scheme 1. Caproic acid.

Co(II), Ni(II), Zn(II), ZrO(II), UO_2(II), Zr(IV) and Th(IV) metal ions and the products were characterized. The thermal stabilities and the kinetic parameters data were calculated as well as the antibacterial screening of these complexes and the free ligand against different bacterial species has been reported.

2. Experimental

2.1. Materials and instrumentation

All chemicals were reagent grade and were used without further purification. Caproic acid was purchased from Fluka Chemical Co., $CrCl_3{\cdot}6H_2O$, $MnCl_2{\cdot}4H_2O$, $FeCl_3$, $CoCl_2{\cdot}6H_2O$, $NiCl_2{\cdot}6H_2O$, $ZnBr_2$, $ZrOCl_2{\cdot}6H_2O$, $UO_2(NO_3)_2{\cdot}6H_2O$, $ZrCl_4$ and $ThCl_4$ from (Merck Co.).

Carbon and hydrogen contents were determined using a Perkin-Elmer CHN 2400 in the Micro-analytical Unit at the Faculty of Science, Cairo University, Egypt. The metal content was found gravimetrically by converting the compounds into their corresponding oxides.

IR spectra were recorded on Bruker FTIR Spectrophotometer (4000–400 cm^{-1}) in KBr pellets. The UV–vis, spectra were determined in the DMSO solvent with concentration (1.0×10^{-3} M) for the caproic acid and their ten complexes using Jenway 6405 Spectrophotometer with 1cm quartz cell, in the range 800–200 nm. Molar conductivities of freshly prepared 1.0×10^{-3} mol/dm^{-3} DMSO solutions were measured using Jenway 4010 conductivity meter.

Magnetic measurements were carried out on a Sherwood Scientific magnetic balance in the micro analytical laboratory, faculty of science, Mansoura University, Egypt using Gouy method.

2.1.1. Calibration

Two very good solid calibrants are used: $Hg[Co(CNS)_4]$ and $[Ni(en)_3](S_2O_3)$. They are easily prepared pure, do not decompose or absorb moisture and pack well. Their susceptibilities at 20 °C are 16.44×10^{-6} and 11.03×10^{-6} c.g.s. Units, decreasing by 0.05×10^{-6} and 0.04×10^{-6} per degree temperature raise respectively, near room temperature. The cobalt compound, besides having the higher susceptibility, also packs rather densely and is suitable for calibrating low fields, while the nickel compound with lower susceptibility and density is suitable for higher field [23]. Here we are used $Hg[Co(CNS)_4]$ only as calibrant.

^1H NMR spectrum of the free acid, Zn^{2+}, Fe^{3+} and Th^{4+} complexes were recorded on Varian Gemini 200 MHz spectrometer using DMSO-d_6 as solvent and TMS as an internal reference. Thermogravimetric analysis (TGA and DTG) were carried out in dynamic nitrogen atmosphere (30 ml/min) with a heating rate of 10 C/min using a Schimadzu TGA-50H thermal analyzer.

2.2. Synthesis of metal complexes

2.2.1. $[Cr(cap)_3]{\cdot}5H_2O$ (**I**, $C_{18}H_{43}O_{11}Cr$) complex

Caproic acid (3.0 mmol) was added to 30 ml methanol and titrated against methanolic sodium hydroxide (0.1 M) to adjust pH at 7.0, then 10 ml methanolic solution of (0.266 g, 1.0 mmol) of $CrCl_3{\cdot}6H_2O$ was added with continuously stirring, after that the mixture was warmed at about ~60 °C and then neutralized. Immediately, the black blue precipitate was settle down and filtered off, washed several times by minimum amounts of hot methanol and dried under *vacuo* over anhydrous $CaCl_2$.

2.2.2. $[Mn(cap)_2(H_2O)_2]$ (**II**, $C_{12}H_{26}O_6Mn$) complex

A similar procedure as that described for complex (**I**) was carried out, by mixing (2.00 mmol) of caproic acid with $MnCl_2{\cdot}2H_2O$ (0.198 g, 1.0 mmol).

2.2.3. $[Fe(cap)_3]{\cdot}12H_2O$ (**III**, $C_{18}H_{57}O_{18}Fe$) complex

A brown complex, $[Fe(cap)_3]{\cdot}12H_2O$ was prepared during the reaction of (3 mmol) caproic acid with (0.162 g, 1.0 mmol) of $FeCl_3$ by a method similar to that used for the preparation of (**I**) complex.

2.2.4. $[Co(cap)_2(H_2O)_2]{\cdot}4H_2O$ (**IV**, $C_{12}H_{34}O_{10}Co$) complex

Exactly, like the above procedure of the preparation of Mn(II) caproate complex. A methanolic solution of $CoCl_2{\cdot}6H_2O$ (0.257 g, 1.0 mmol) was mixed with an equal volume of caproic acid solution (2.0 mmol) in methanol. The mixture was allowed to stays at room temperature for about 1 h with constant stirring and then heated on a water bath at ~60 °C for 30 min. The black green complex was filtered off, washed several times with hot methanol, dried under *vacuo* over anhydrous $CaCl_2$.

2.2.5. $[Ni(cap)_2(H_2O)_2]{\cdot}3H_2O$ (**V**, $C_{12}H_{32}O_9Ni$) complex

The nickel(II) caproate complex was prepared by the same method which used for preparation of the Mn(II) and Co(II) complexes. The weight of $NiCl_2{\cdot}6H_2O$ was (0.256 g, 1.0 mmol) and mixing with caproic acid by (1:2) molar ratio in methanol as solvent.

2.2.6. $[Zn(cap)_2]$ (**VI**, $C_{12}H_{22}O_4Zn$) complex

The complex, $[Zn(cap)_2]$, was prepared by mixing equal volumes (30 ml) of caproic acid (2.0 mmol) with $ZnBr_2$ (0.224 g, 1.0 mmol). The mixture was neutralized by titrated with NaOH to adjust pH at 7.0 and then heated on a water bath at 60 °C with constant stirring for about 45 min. A white solid complex was precipitated and its amount increasing with increasing the time of heating. The obtained precipitate was separated, washed several times with hot methanol and then dried in *vacuo* over anhydrous $CaCl_2$ and recrystalization occurs using a mixture of water and methanol (1:1).

2.2.7. $[ZrO(cap)_2]\cdot 3H_2O$ (**VII**, $C_{12}H_{28}O_8Zr$) and $[UO_2(cap)(NO_3)]$ (**VIII**, $C_6H_{11}NO_7U$) complexes

Preparation of these two complexes followed essentially the same procedure as preparation of (**I**), but the weight of $ZrOCl_2\cdot 6H_2O$ and $UO_2(NO_3)_2\cdot 6H_2O$ were (0.286 g, 1.0 mmol) and (0.502 g, 1.0 mmol), respectively. The pH was adjusted at 7.0.

2.2.8. $[Zr(cap)_2(Cl)_2]$ (**IX**, $C_{12}H_{22}O_4Cl_2Zr$) and $[Th(cap)_4]$ (**X**, $C_{24}H_{44}O_8Th$) complexes

These two complexes, $[Zr(cap)_2(Cl)_2]$ and $[Th(cap)_4]$ were prepared during the reaction of caproic acid with $ZrCl_4$ and $ThCl_4$ at 60 °C, respectively, in (1:4) molar ratio (M^{4+}: cap) by a method similar to that used for the preparation of $[Cr(cap)_3]\cdot 5H_2O$ complex. These complexes were started to settle down as a white precipitate after a 1 h of heating. Separately by filtration, washed several times with hot methanol to remove any residue of caproic acid and then dried in a vacuum dissector over $CaCl_2$ for about 4 days.

2.3. Antibactrial investigation

For these investigations the hole well method was applied. The investigated isolates of bacteria were seeded in tubes with nutrient broth (NB). The seeded NB (1 cm^3) was homogenized in the tubes with 9 cm^3 of melted (45 °C) nutrient agar (NA). The homogeneous suspensions were poured into Petri dishes. The holes (diameter 4 mm) were done in the cool medium. After cooling in these holes, 2×10^{-3} dm^3 of the investigated compounds were applied using a micropipette. After incubation for 24 h in a thermostat at 25–27 °C, the inhibition (sterile) zone diameters (including disc) were measured and expressed mm. An inhibition zone diameter over 7 mm indicates that the tested compound is active against the bacteria under investigation.

The antibacterial activities of the investigated compounds were tested against *Escherichia coli*, *Streptococcus penumonia* and *Bacillus subtilis*. The concentration of each solution was 1.0×10^{-3} mol dm^3. Commercial DMSO was employed to dissolve the tested samples.

3. Results and discussion

The results of the elemental analysis and some physical characteristics of the obtained compounds are given in Table 1.

The complexes are air-stable, hygroscopic, with higher melting points, insoluble in H_2O and most of organic solvents except for DMSO and DMF.

The elemental analysis data (Table 1) of the complexes indicates a 1:1 metal:ligand stoichiometry for $[UO_2(cap)(NO_3)]$ complexes, 1:2 for $[Mn(cap)_2(H_2O)_2]$, $[Co(cap)_2(H_2O)_2]\cdot 4H_2O$, $[Ni(cap)_2(H_2O)_2]\cdot 3H_2O$, $[Zn(cap)_2]$, $[ZrO(cap)_2]\cdot 3H_2O$, and $[Zr(cap)_2(Cl)_2]$, 1:3 for $[Cr(cap)_3]\cdot 5H_2O$ and $[Fe(cap)_3]\cdot 12H_2O$ and 1:4 for $[Th(cap)_4]$.

3.1. Molar conductivities of metal chelates

The molar conductivity values for the caproate complexes in DMSO solvent (1.0×10^{-3} mol) were in the range (9.64–31.80) Ω^{-1} cm^{-1} mol^{-1}, suggesting them to be non-electrolytes nature (Table 1). Conductivity measurements have frequently been used in structural of metal chelates (mode of coordination) within the limits of their solubility. They provide a method of testing the degree of ionization of the complexes, the molecular ions that a complex liberates in solution (incase of presence anions outside the coordination sphere), the higher will be its molar conductivity and vice versa [24]. It is clear from the conductivity data that the complexes present seem to be non-electrolytes. Also the molar conductance values indicate that the anions may be exhibits inside the coordination sphere as in $[UO_2(cap)(NO_3)]\cdot H_2O$ and $[Zr(cap)_2(Cl)_2]$ complexes or absent as found in the others. This results were strongly supported with the chemical analysis (elemental analysis data) where Cl^- ions are not detected by addition of $AgNO_3$ solution, this tested well matched with CHN data, but in the case of $[Zr(cap)_2(Cl)_2]$ complex, the chloride ion can be detected inside the coordination sphere of the complex by the degradation of the complex using nitric acid.

3.2. Infrared spectra

The main IR data are summarized in Table 2. Caproic acid exhibits a strong absorption band at 1711 cm^{-1} due to the

Table 1
Elemental analyses and physical data of the caproate complexes

Compounds	Molecular weight	mp (°C)	Color	Content ((calculated) found)				Λm (Ω^{-1} cm^{-1} mol^{-1})
				% C	% H	% N	%M	
$[Cr(cap)_3]\cdot 5H_2O$ (**I**, $C_{18}H_{43}O_{11}Cr$)	486.99	>300	Black-blue	(44.35) 43.09	(8.83) 8.63	–	(10.67) 10.33	24.30
$[Mn(cap)_2(H_2O)_2]$ (**II**, $C_{12}H_{26}O_6Mn$)	320.94	220	Brown	(44.87) 43.37	(8.10) 7.26	–	(17.12) 17.08	18.70
$[Fe(cap)_3]\cdot 12H_2O$ (**III**, $C_{18}H_{57}O_{18}Fe$)	616.85	260	Brown	(35.01) 34.68	(9.24) 8.92	–	(9.05) 8.95	23.04
$[Co(cap)_2(H_2O)_2]\cdot 4H_2O$ (**IV**, $C_{12}H_{34}O_{10}Co$)	396.93	>300	Black-green	(36.27) 35.94	(8.56) 8.47	–	(14.84) 14.77	31.80
$[Ni(cap)_2(H_2O)_2]\cdot 3H_2O$ (**V**, $C_{12}H_{32}O_9Ni$)	378.70	>300	Pall-green	(38.02) 36.96	(8.44) 8.36	–	(15.50) 13.79	30.10
$[Zn(cap)_2]$ (**VI**, $C_{12}H_{22}O_4Zn$)	295.38	160	White	(48.75) 48.43	(7.44) 7.31	–	(22.13) 21.98	9.80
$[ZrO(cap)_2]\cdot 3H_2O$ (**VII**, $C_{12}H_{28}O_8Zr$)	391.22	>300	White	(36.80) 35.62	(7.15) 7.09	–	(23.31) 23.24	23.80
$[UO_2(cap)(NO_3)]$ (**VIII**, $C_6H_{11}NO_7U$)	447.03	>300	Yellow	(16.11) 15.27	(2.46) 2.41	(3.13) 3.07	(53.24) 53.27	14.34
$[Zr(cap)_2(Cl)_2]$ (**IX**, $C_{12}H_{22}O_4Cl_2Zr$)	392.22	>300	White	(36.71) 36.96	(5.61) 5.48	–	(23.26) 23.73	12.18
$[Th(cap)_4]$ (**X**, $C_{24}H_{44}O_8Th$)	692.04	>300	White	(41.62) 41.32	(6.36) 5.93	–	(33.53) 33.46	9.64

Table 2
IR frequencies (cm^{-1}) of coproic acid (Hcap) and its metal complexes

Assignments	Compound											
	Hcap	I	II	III	IV	V	VI	VII	VIII	IX	X
ν(OH); H_2O	–	3445	3421	3422	3424	3418	–	3421	3446	–	–
ν_{as}(CH)	2959, 2935	2958, 2930	2958, 2929	2959, 2929	2957, 2929	2957, 2930	2956, 2927	2957, 2930	2957, 2929	2957, 2929	2958, 2930
ν_s(CH)	2875, 2864	2865, 2823	2866	2866	2864	2866	2865	2867	2863	2868	2866
ν(COOH)	1711	–	–	–	–	–	–	–	–	–	–
ν_{as}(COO^-)	–	1534	1555	1542	1554	1564	1533	1559	1532	1568	1515
δ(CH)	1468, 1414	1450	1415	1439	1410	1418	1458, 1402	1451	1465	1447	1453
ν_s(COO^-)	–	1319	1342, 1316	1317	1313	1342, 1316	1346	1318	1319	1344, 1319	1339, 1314
ν_{as}(CC)	1213, 1114, 1107	1227, 1186, 1110	1227, 1190, 1109	1225, 1188, 1109	1225, 1187, 1108	1225, 1190, 1108	1231	1225, 1189, 1109	1227, 1192, 1107	1226, 1189, 1108	1224, 1190, 1106
ν_s(CC)	937	916	950	983	1045	1055	958	961	927	961	958
δ(CC)	732	794, 735	730	–	732	730	741	730	–	733	724
ν(M–O)	–	421	420	486	410	422	458	459	480	473	421

free carboxylic C=O group. This group disappeared in the spectra of their complexes. Interestingly, there are two bands appeared at the range of 1515–1568 cm^{-1} which corresponding to $\nu_{as}(COO^-)$ and the other band is exhibited within the range 1313–1346 cm^{-1} assigned to $\nu_s(COO^-)$.

Dependently, the antisymmetric and symmetric stretching vibration modes ($\nu_{as}(COO^-)$, and $\nu_s(COO^-)$) of the COO^- group, the structure of our complexes can be elucidated [25]. The direction of the frequency shift of the $\nu_{as}(COO^-)$ and the $\nu_s(COO^-)$ bands with respect to those of the free ion depends on the coordination mode of the COO^- group with the metal ion. There are three principle modes of coordination as shown in Scheme 2.

Nakamoto and McCarthy [26] have established that if the coordination is monodentate (structure a) the $\nu_{as}(COO^-)$ and $\nu_s(COO^-)$ will be shifted to higher and lower frequencies, respectively. Whereas, if the coordination is chelating bidentate (structure b) or bridging bidentate (structure c) both $\nu_{as}(COO^-)$ and $\nu_s(COO^-)$ frequencies will change in the same direction because the bond orders of both C=O bonds would change by the same amount. Based on these facts and comparison the $\nu_{as}(COO^-)$ and $\nu_s(COO^-)$ frequencies of our caproate complexes by the $\nu_{as}(COO^-)$ and $\nu_s(COO^-)$ frequencies of sodium carboxylate [27], as shown in Table 3, we can say that: all of the resulted complexes are chelating bidentate structure.

The stretching broad band vibration of OH^- group ν(O–H) is occurred as expected [28] at the range 3418–3445 cm^{-1}. The angular deformation motions of the coordinated water in the hydrated caproate complexes can be classified into four types of vibrations: δ_b(bend), δ_r(rock), δ_t(twist) and δ_w(wag).

The assignments of these motions in $[Mn(cap)_2(H_2O)_2]$, $[Co(cap)_2(H_2O)_2]\cdot 4H_2O$ and $[Ni(cap)_2(H_2O)_2]\cdot 3H_2O$ complexes., are as follows. The bending motion, $\delta_b(H_2O)$, is assigned to its characteristic band around at ~1630 cm^{-1} (shoulder band). The rocking motions, $\delta_r(H_2O)$, is assigned at 730 cm^{-1} and the wagging motion, $\delta_w(H_2O)$, is observed at ~600 cm^{-1}. The twisting motion, $\delta_t(H_2O)$, is observed at above 620 cm^{-1}. It should be mentioned here that these assignments for both the bond stretches and angular deformation of the coordinated water molecules fall in the frequency regions reported for related complexes [26].

The characteristic stretching vibrations of the bidentate nitrato group, NO_3^-, in the $[UO_2(cap)(NO_3)]$ complex is observed at 1375 cm^{-1} (shoulder peak) attributed to $\nu(NO_2)$ [26]. The stretching motion of (ν(N=O)) is observed at 1465 cm^{-1} as a very strong band combined with δ(CC) vibration motion in the same place, while the two bending motion of the type $\delta(NO_2)$ are well resolved and observed at 750 and 653 cm^{-1} as weak shoulder and weak bands, respectively.

The ν(U=O) vibration in the uranyl complex is observed as expected as a strong band at 928 cm^{-1} is a good agreement with those known for many dioxouranium(VI) complexes [26]. On the other hand concerning, the infrared spectra of $[ZrO]^{2+}$ complex show a medium absorption band at 1109 cm^{-1} due to ν(Zr=O) as expected [26].

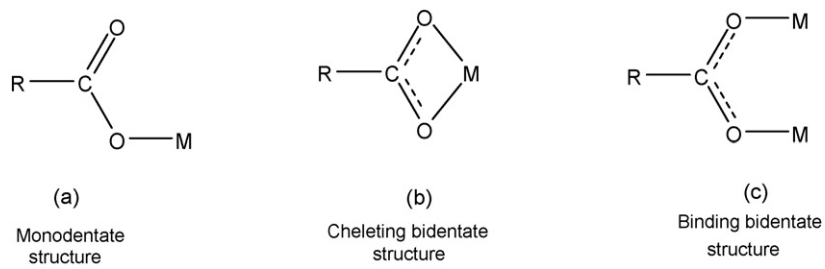

Scheme 2. Possible coordination features of the carboxylate group.

Table 3
Asymmetric and symmetric stretching vibrations of the carboxylate group

Compound	$\nu_{as}(COO^-)$	$\nu_s(COO^-)$	$\Delta\nu = \nu_{as}(COO^-) - \nu_s(COO^-)$	Bonding mode
Hacap	1565	1425	140	Bidentate
$[Cr(cap)_3]\cdot 5H_2O$	1534	1319	215	Bidentate
$[Mn(cap)_2(H_2O)_2]$	1555	1342	213	Bidentate
$[Fe(cap)_3]\cdot 12H_2O$	1542	1316	226	Bidentate
$[Co(cap)_2(H_2O)_2]\ 4H_2O$	1554	1313	241	Bidentate
$[Ni(cap)_2(H_2O)_2]\ 3H_2O$	1564	1342	222	Bidentate
$[Zn(cap)_2]$	1533	1346	187	Bidentate
$[ZrO(cap)_2]\cdot 3H_2O$	1559	1318	241	Bidentate
$[UO_2(cap)(NO_3)]$	1532	1319	213	Bidentate
$[Zr(cap)_2(Cl)_2]$	1568	1344	224	Bidentate
$[Th(cap)_4]$	1515	1339	176	Bidentate

3.3. Magnetic measurements

Magnetic measurements were carried out on a Sherwood Scientific magnetic balance according to the Gauy method. The calculations were evaluated by applying the following equations:

$$\chi_g = \frac{cl(R-R_0)}{10^9 M}, \qquad \chi_m = \chi_g MWt, \qquad \mu_{eff} = 2.828\sqrt{\chi_m T}$$

where χ is mass susceptibility per g sample; c is the calibration constant of the instrument and equal to 1.135; R is the balance reading for the sample and tube; R_0 is the balance reading for the empty tube; M is the weight of the sample in g; T is the absolute temperature.

The magnetic moments of the Cr(III), Mn(II), Fe(III), Co(II) and Ni(II) caproate complexes at $T = 300$ K and their corresponding hybrid orbitals are given in Table 4.

From the data were represented in Table 4, the observed values of the effective magnetic moments μ_{eff} operated for above complexes are convenient with experimental values [29] obtained for high spin octahedral for all mentioned complexes under investigation except for Mn(II) and Fe(III) caproate complexes which are low spin octahedral configuration.

3.4. Electronic absorption spectra

The spectra of the caproic acid complexes in DMSO are shown in Fig. 1 and the spectral data are listed in Table 5.

There are two detected absorption bands at around 225 and 265 nm assigned to π–π* and n–π* intraligand transitions, respectively, in the electronic spectrum of the ligand. These transitions also found in the spectra of the complexes, but they are shifted, confirming the coordination of the ligand to the metallic ions. The first band around 225 nm is probably due to a π–π* of the alkyl group. However, the second band around 265 nm is due to presence of COOH group [30]. In case of our complexes, the carboxylic group is blue shifted. This result confirms the complexation of metal ions via carboxylic group. Some complexes have a band at range 270–415 nm may be assigned to the ligand to metal charge-transfer [31,32]. The broad band which appears at 575 in the spectrum of Cr(II) caproate complex can be attributed to d–d transition.

Table 4
Magnetic moment of the Cr(III), Mn(II), Fe(III), Co(II) and Ni(II) complexes

Complex	μ_{eff} B.M. (found)	μ_{eff} B.M. (calc.)	Hybrid orbitals	Stereo-chemistry
$[Cr(cap)_3]\cdot 5H_2O$	3.35	3.77	d^2sp^3	Octahedral
$[Mn(cap)_2(H_2O)_2]$	1.76	2.18	d^2sp^3	Octahedral
$[Fe(cap)_3]\cdot 12H_2O$	2.20	2.25	d^2sp^3	Octahedral
$[Co(cap)_2(H_2O)_2]\cdot 4H_2O$	1.74	1.88	d^2sp^3	Octahedral
$[Ni(cap)_2(H_2O)_2]\cdot 3H_2O$	2.82	3.89	sP^3d^2	Octahedral

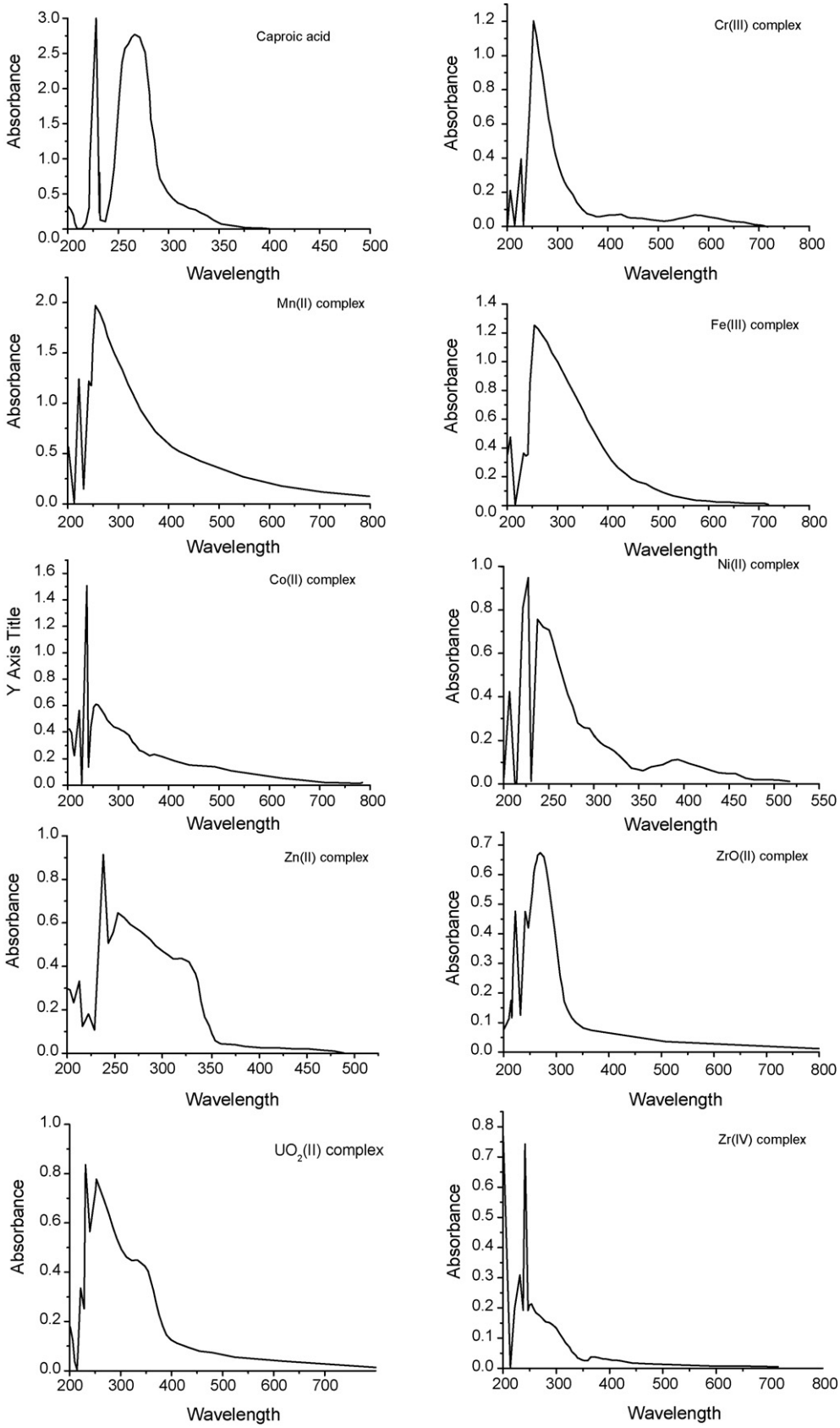

Fig. 1. The UV spectra of caproic acid and their complexes.

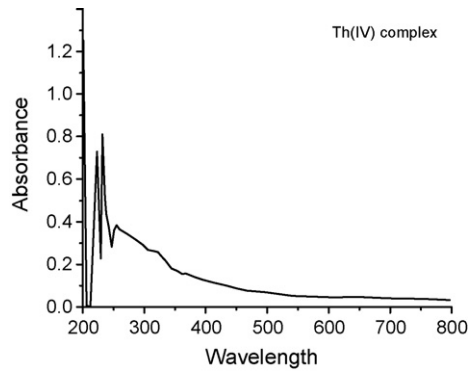

Fig. 1. (*Continued*).

3.5. ^1H NMR spectra

The ^{1}H NMR spectral data of the Zn^{2+}, Fe^{3+} and Th^{4+} complexes and the free ligand (Hcap) caproic acid are collected in Table 6 and their spectra are shown in Fig. 2. The Zn(II), Fe(III) and Th(IV) complexes appear to binding to the caproic acid through carboxylate group, the absence of proton of (COOH) confirm the mode of coordination.

Table 5
The electronic spectral date of the free ligand and its complexes

Compound	λ_{max} (nm)	ε (mol^{-1} cm^{-1})	Assignment
Hacap	225	3000	π–π* trans.
	265	2784	n–π* trans.
$[Cr(cap)_3]\cdot 5H_2O$	225	409	π–π* trans.
	250	1203	n–π* trans.
	415	70	L → Cr C.T.
	575	69	d–d trans.
$[Mn(cap)_2(H_2O)_2]$	220	1225	π–π* trans.
	255	1965	n–π* trans.
$[Fe(cap)_3]\cdot 12H_2O$	230	371	π–π* trans.
	255	1259	n–π* trans.
$[Co(cap)_2(H_2O)_2]\cdot 4H_2O$	220	602	π–π* trans.
	235	1594	π–π* trans.
	255	662	n–π* trans.
	335	300	L → Co C.T.
$[Ni(cap)_2(H_2O)_2]\cdot 3H_2O$	225	960	π–π* trans.
	240	776	n–π* trans.
	395	104	L → Ni C.T.
$[Zn(cap)_2]$	220	191	π–π* trans.
	235	913	π–π* trans.
	250	646	n–π* trans.
	320	420	L → Zn C.T.
$[ZrO(cap)_2]\cdot 3H_2O$	220	480	π–π* trans.
	240	482	n–π* trans.
	270	677	n–π* trans.
$[UO_2(cap)(NO_3)]$	220	337	π–π* trans.
	230	837	π–π* trans.
	250	774	n–π* trans.
	350	425	L → U C.T.
$[Zr(cap)_2(Cl)_2]$	230	310	π–π* trans.
	240	740	π–π* trans.
	250	218	n–π* trans.
	365	40	L → Zr C.T.
$[Th(cap)_4]$	220	726	π–π* trans.
	230	814	π–π* trans.
	250	396	n–π* trans.
	322	257	L → Th C.T.

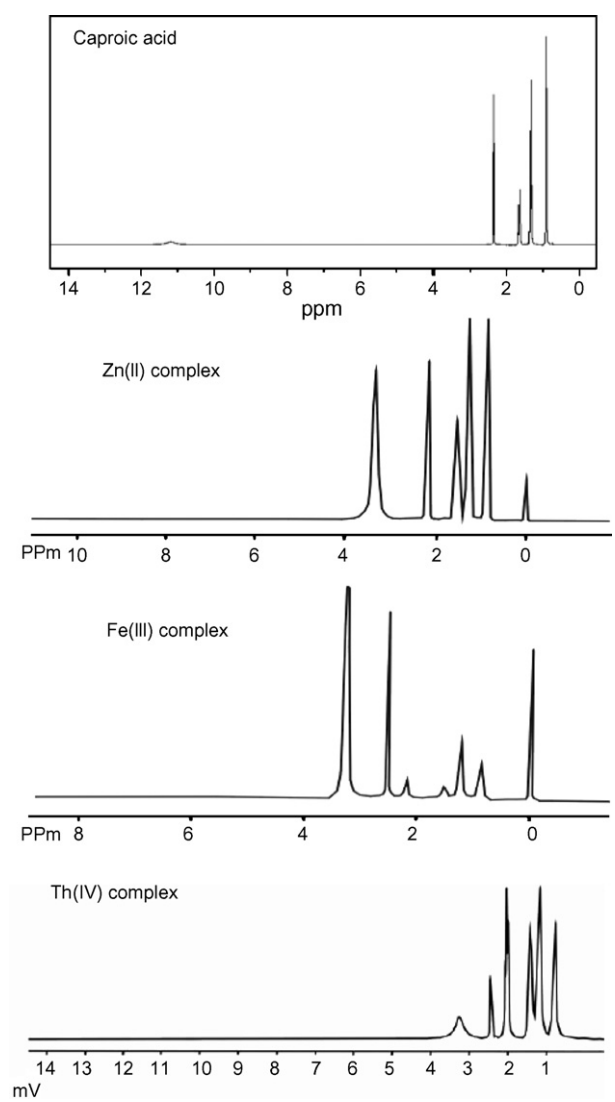

Fig. 2. The ^{1}H NMR spectra of caproic acid, Zn(II), Fe(III) and Th(IV) complexes.

Table 6
The ^{1}H NMR spectral data[a] (δ, ppm)[b] of the caproic acid and their complexes

Compound	$-CH_2$ (C_2)	$-CH_2$ (C_3)	$-CH_2$ and $-CH_2$ (C_4 and C_5)	$-CH_3$ (C_6)	Proton of COOH
Hcap	2.35	1.64	1.33	0.90	11.20
$[Zn(cap)_2]$	2.12	1.57	1.28	0.88	–
$[Fe(cap)_3]\cdot 12H_2O$	2.20	1.55	1.28	0.89	–
$[Th(cap)_4]$	2.42	2.05	1.40	0.78	–

[a] Solvent DMSO-d_6.
[b] Relative to TMS.

3.6. Thermogravimetric analysis

Thermal analysis curves (TG and DTG) of the studies complexes are shown in Fig. 3. The thermoanalytical results are summarized in Table 7.

3.6.1. $[Cr(cap)_3]\cdot 5H_2O$

The thermal decomposition of this complex occurs at two steps. The first degradation step take place in the range of 30–450 °C and it is corresponds to the eliminated of all five uncoordinated water molecules beside of organic moiety (C_6H_{12}) due to a weight loss of 35.18% in a good matching with theoretical value 35.69%. The second step fall in the range of 450–800 °C which is assigned to loss of $C_6H_{21}O_{4.5}$ (remaining organic moiety) with a weight loss 34.78% and the calculated value is 33.84%. The Cr_2O_3 is the final product remains stable till 800 °C. Reported data dealing in the thermal analysis investigation within nitrogen atmosphere indicate that, the Cr(III) complex decompose to give oxide contaminated with few carbon atoms as final products, this reason, because of limited supply of oxygen.

3.6.2. $[Mn(cap)_2(H_2O)_2]$

The thermal decomposition of $[Mn(cap)_2(H_2O)_2]$ complex completely in two steps. The first step ranged at 30–375 °C corresponding to the loss of $2H_2O$ molecules and $C_8H_{22}O$ organic molecule, representing a weight loss of 53.23% and its calculated value is 52.97%. The second step occurring at 375–800 °C

Table 7
Thermal data of the caproate complexes

Compound	Steps	Temperature range (°C)	DTG peak (°C)	TG weight loss (%)		Assignments
				Calc.	Found	
$[Cr(cap)_3]\cdot 5H_2O$	1st	30–450	298	35.69	35.18	$5H_2O + C_6H_{12}$ (organic moiety)
	2nd	450–800	507	33.84	34.78	$C_6H_{21}O_{4.5}$ (organic moiety)
				30.47	30.04	$1/2Cr_2O_3 + 6C$ (residue)
$[Mn(cap)_2(H_2O)_2]$	1st	30–375	300	52.97	53.23	$2H_2O + C_8H_{22}O$ (organic moiety)
	2nd	375–800	455	8.72	8.89	CO
				38.31	37.88	$MnO_2 + 3C$ (residue)
$[Fe(cap)_3].12H_2O$	1st	30–500	262	52.04	51.76	$16.5H_2O + 12H_2$ (organic moiety)
				47.96	48.24	$1/2Fe_2O_3 + 18C$ (residue)
$[Co(cap)_2(H_2O)_2]\cdot 4H_2O$	1st	30–225	71	18.14	17.86	$4H_2O$
	2nd	225–550	364	26.70	24.84	$2H_2O + 11H_2 + 3/2O_2$ (organic moiety)
				55.16	57.30	$CoO + 12C$ (residue)
$[Ni(cap)_2(H_2O)_2]\cdot 3H_2O$	1st	30–550	319	61.27	60.54	$5H_2O + C_6H_{22}O_3$ (organic moiety)
				38.73	39.46	$NiO + 6C$ (residue)
$[Zn(cap)_2]$	1st	50–450	310	72.37	72.65	$C_{12}H_{22}O_3$ (organic moiety)
				27.52	25.35	ZnO (residue)
$[ZrO(cap)_2]\cdot 3H_2O$	1st	30–250	193	13.80	13.48	$3H_2O$
	2nd	250–800	324	39.37	40.59	$C_7H_{22}O_3$ (organic moiety)
				46.83	45.93	$ZrO_2 + 5C$ (residue)
$[UO_2(cap)(NO_3)]$	1st	30–500	290	23.48	23.45	$11/2H_2 + 3/2O_2 + NO_2$ (organic moiety)
				76.52	76.55	$UO_2 + 6C$ (residue)
$[Zr(cap)_2(Cl)_2]$	1st	30–225	174	14.79	15.50	C_4H_{10} (organic moiety)
	2nd	225–600	346	38.49	38.95	$C_3H_{12}O_2 + Cl_2$ (organic moiety)
				46.72	45.55	$ZrO_2 + 5C$ (residue)
$[Th(cap)_4]$	1st	30–450	271	61.85	63.13	$C_{24}H_{44}O_6$ (organic moiety)
				38.15	36.87	ThO_2 (residue)

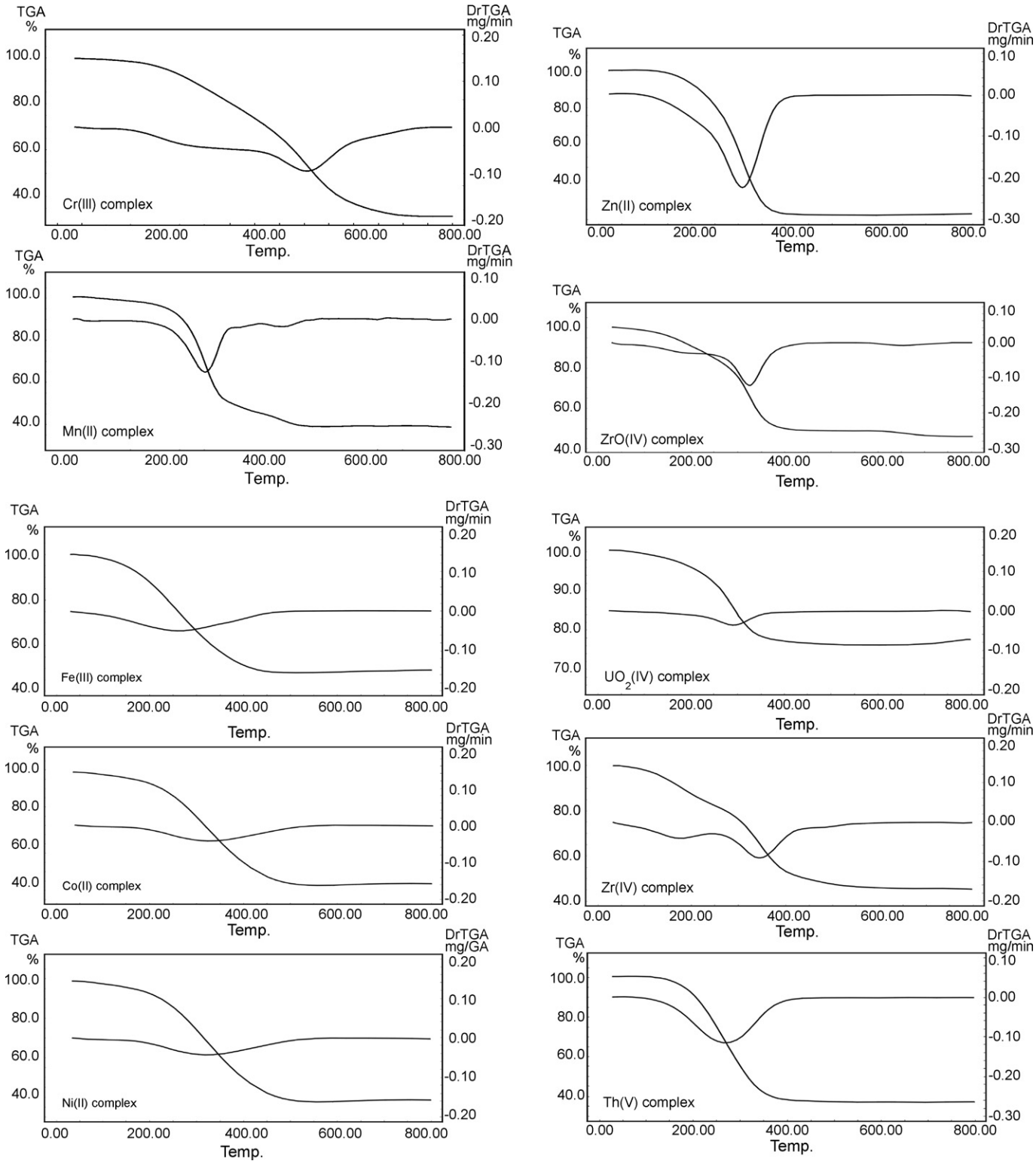

Fig. 3. The TG and DTG of the caproate complexes.

corresponding to the loss of CO molecule, representing a weight loss of 8.89% and its calculated value is 8.72%. This step can be interpreted according to the transform of $MnCO_3$ to MnO_2.

3.6.3. $[Fe(cap)_3]\cdot 12H_2O$

The ferric(III) caproate complex decomposed in only one step which extended from 30 to 500 °C and can be assigned to the loss of $16.5H_2O$ molecules and $12H_2$ molecules, representing a

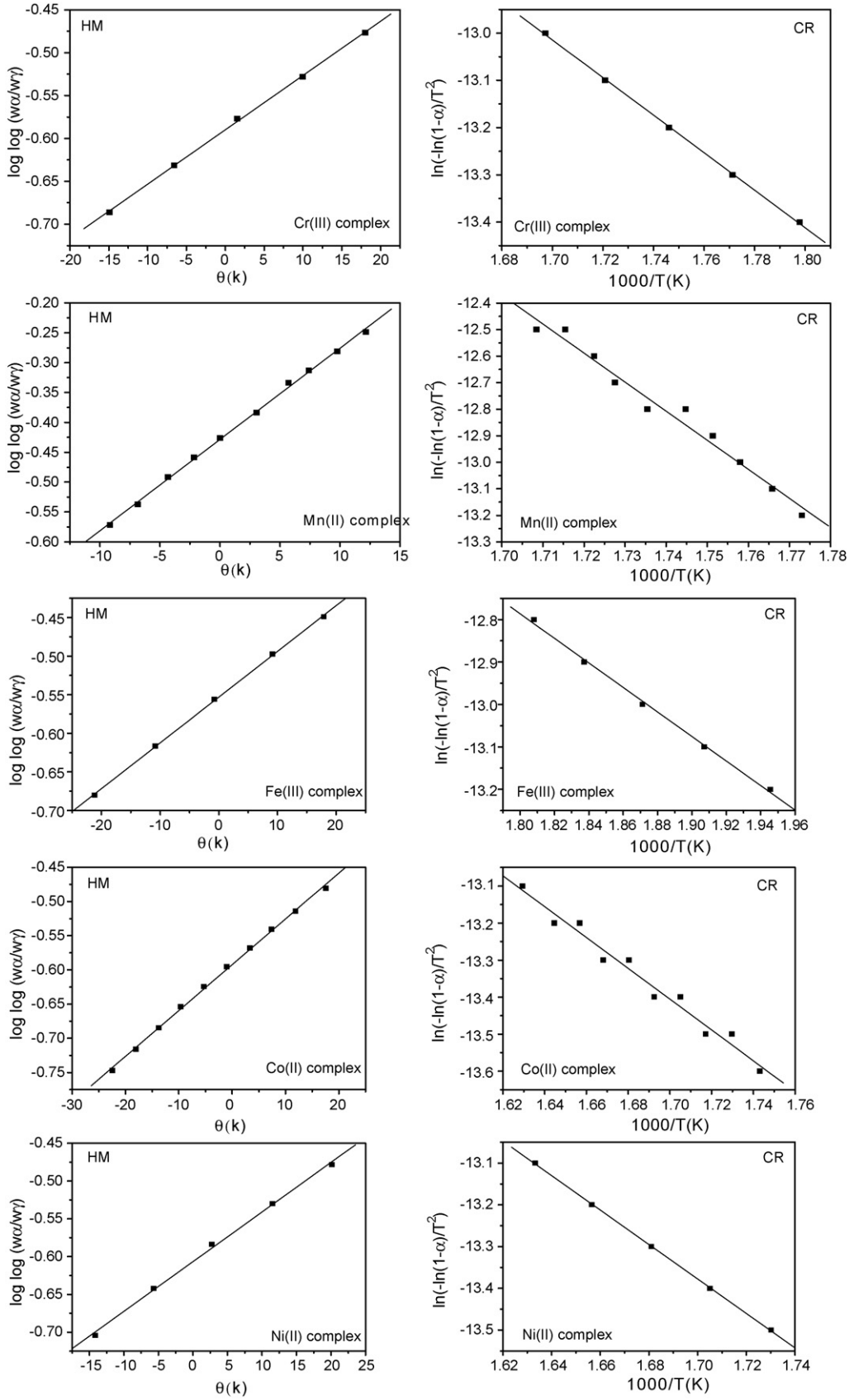

Fig. 4. Horowitz–Metzger (HM), Coats–Redfern (CR) of the first step of the caproate complexes.

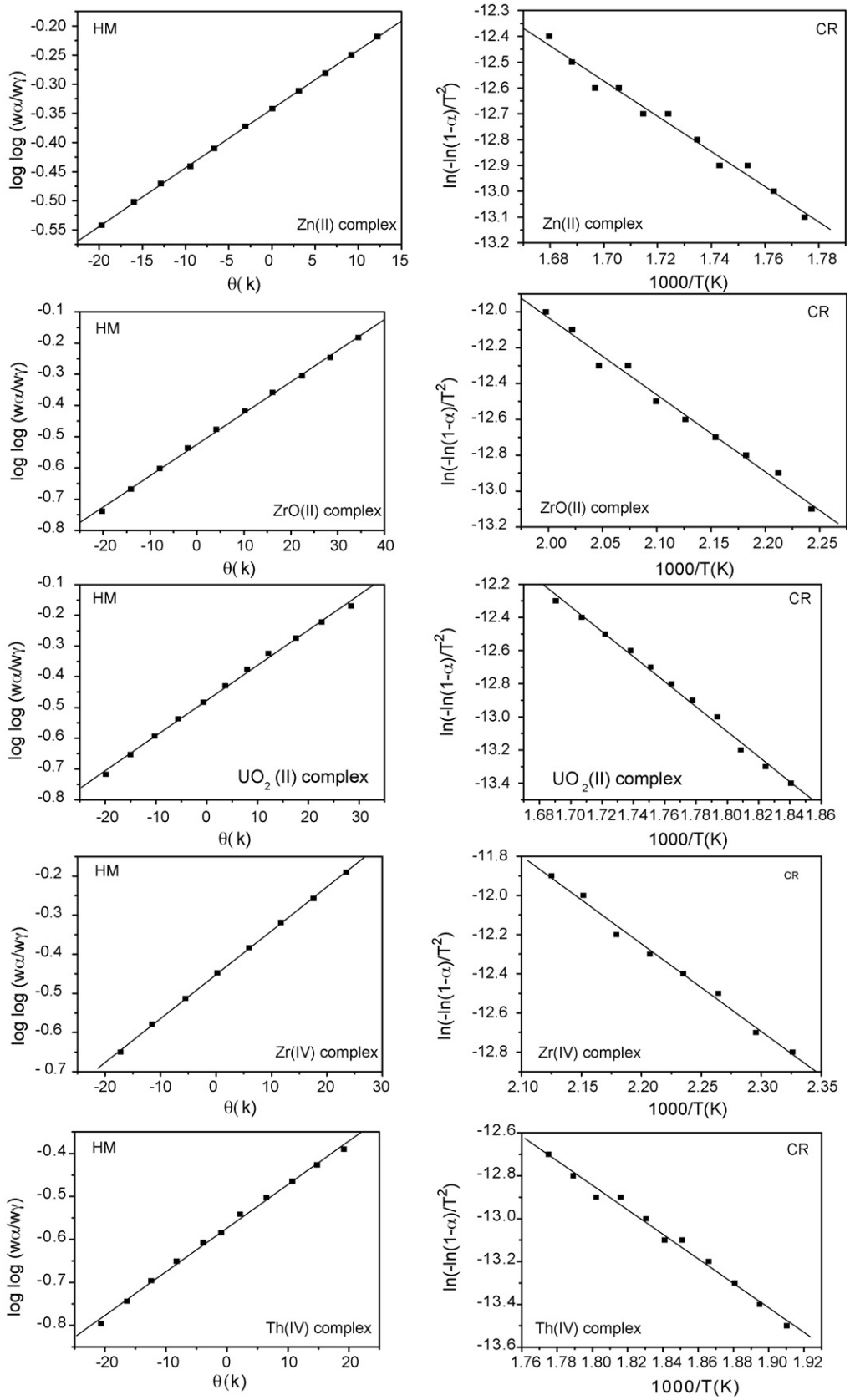

Fig. 4. (*Continued*).

weight loss of 51.76% and its calculated value is 52.04%. The final products resulted at 800 °C contain Fe_2O_3 polluted with carbon atoms.

3.6.4. $[Co(cap)_2(H_2O)_2]\cdot 4H_2O$

To make sure about the proposed formula and structure for the new cobalt(II) complex, $[Co(cap)_2(H_2O)_2]\cdot 4H_2O$, thermo gravimetric (TG) and differential thermo gravimetric analysis (DTG) was carried out for this complex under N_2 flow. DTG thermogram is shown in Fig. 3. The thermal decomposition of the cobalt(II) complex proceeds approximately with main two degradation steps. The first stage occurs at maximum temperature of 71 °C. The weight loss associated with this stage 17.86% which is very close to the theoretical value of 18.14% corresponding to the loss of $4H_2O$ as will be described in Table 7. The second step occurring at 225–550 °C is corresponding to

Table 8
Kinetic parameters using the Coats–Redfern (CR) and Horowitz–Metzger (HM) operated for the caproate complexes

Complex	Stage	Method	Parameter					r
			E (J mol^{-1})	A (s^{-1})	ΔS (J mol^{-1} K^{-1})	ΔH (J mol^{-1})	ΔG (J mol^{-1})	
I	1st	CR	3.30×10^4	5.19×10^5	-1.41×10^2	2.83×10^4	1.09×10^5	0.9997
		HM	3.95×10^4	1.51×10^3	-2.28×10^2	4.48×10^4	1.65×10^5	0.9997
		Average	3.62×10^4	2.60×10^4	-1.84×10^2	3.65×10^5	1.37×10^5	
	2nd	CR	8.70×10^4	4.65×10^3	-1.85×10^2	8.05×10^4	2.25×10^5	0.9989
		HM	8.53×10^4	2.17×10^3	-1.89×10^2	7.88×10^4	2.26×10^5	0.9988
		Average	8.62×10^4	3.41×10^3	-1.87×10^2	7.96×10^4	2.25×10^5	
II	1st	CR	9.10×10^4	1.41×10^6	-1.33×10^2	8.63×10^4	1.52×10^5	0.9892
		HM	9.61×10^4	4.98×10^6	-1.22×10^2	9.13×10^4	1.61×10^5	0.9992
		Average	9.53×10^4	3.19×10^6	-1.27×10^2	8.88×10^4	1.56×10^5	
	2nd	CR	2.27×10^5	2.27×10^{14}	22.50	2.20×10^5	2.04×10^5	0.9973
		HM	2.20×10^5	4.55×10^{13}	09.13	2.14×10^5	2.08×10^5	0.9967
		Average	2.23×10^5	1.35×10^{14}	15.81	2.17×10^5	2.05×10^5	
III	1st	CR	2.40×10^4	1.42×10^6	-1.32×10^2	1.96×10^4	9.02×10^4	0.9986
		HM	3.25×10^4	5.10×10^{10}	-2.36×10^2	2.81×10^4	1.54×10^5	0.9998
		Average	2.82×10^5	2.55×10^{10}	-1.84×10^2	2.38×10^4	1.22×10^5	
IV	1st	CR	4.95×10^4	4.48×10^4	-1.57×10^2	4.66×10^4	1.01×10^5	0.9838
		HM	5.41×10^4	2.26×10^6	-1.24×10^2	5.13×10^4	9.41×10^4	0.9808
		Average	5.18×10^4	1.15×10^6	-1.40×10^2	4.89×10^4	9.75×10^5	
	2nd	CR	7.60×10^4	7.06×10^3	-1.78×10^2	7.07×10^4	1.84×10^5	0.9949
		HM	8.79×10^4	1.05×10^5	-1.55×10^2	8.26×10^4	1.81×10^5	0.9992
		Average	8.23×10^4	5.60×10^4	-1.66×10^2	7.66×10^4	1.82×10^5	
V	1st	CR	3.43×10^4	59.80	-2.23×10^2	2.94×10^4	1.12×10^5	0.9993
		HM	4.41×10^4	29.40	-2.23×10^2	3.92×10^4	1.71×10^5	0.9989
		Average	3.92×10^4	44.60	-2.23×10^2	3.43×10^4	1.41×10^5	
VI	1st	CR	5.67×10^4	4.58×10^3	-1.80×10^2	5.18×10^4	1.57×10^5	0.9905
		HM	6.56×10^4	4.39×10^3	-1.81×10^2	6.08×10^4	1.66×10^5	0.9999
		Average	6.11×10^4	4.48×10^3	-1.80×10^2	5.63×10^4	1.61×10^5	
VII	1st	CR	3.58×10^4	3.32×10^4	-1.62×10^2	3.19×10^4	1.07×10^5	0.9942
		HM	4.17×10^4	2.71×10^2	-2.02×10^2	3.78×10^4	1.32×10^5	0.9993
		Average	3.86×10^4	1.67×10^4	-1.82×10^2	3.48×10^4	1.19×10^4	
	2nd	CR	9.33×10^4	8.05×10^5	-1.83×10^2	8.83×10^4	1.71×10^5	0.9951
		HM	9.86×10^4	3.50×10^6	-1.25×10^2	9.36×10^4	1.69×10^5	0.9975
		Average	9.59×10^4	2.15×10^6	-1.54×10^2	9.09×10^4	1.70×10^5	
VIII	1st	CR	6.27×10^4	3.09×10^3	-1.83×10^2	5.85×10^4	1.61×10^5	0.9971
		HM	6.95×10^4	1.85×10^4	-1.68×10^2	6.48×10^4	1.60×10^5	0.9986
		Average	6.61×10^4	1.07×10^4	-1.75×10^2	6.16×10^5	1.6×10^5	
IX	1st	CR	3.72×10^4	1.23×10^4	-1.70×10^2	3.35×10^4	1.10×10^5	0.9960
		HM	4.30×10^4	6.73×10^2	-1.94×10^2	3.92×10^4	1.26×10^5	0.9998
		Average	4.01×10^4	6.48×10^3	-1.82×10^2	3.63×10^4	1.18×10^5	
	2nd	CR	5.41×10^4	2.29×10^4	-1.68×10^2	4.90×10^4	1.53×10^5	0.9915
		HM	6.80×10^4	2.89×10^3	-1.85×10^2	6.28×10^4	1.77×10^5	0.9990
		Average	6.10×10^4	1.28×10^4	-1.76×10^2	5.59×10^4	1.65×10^5	
X	1st	CR	4.75×10^5	1.84×10^4	-1.68×10^2	4.30×10^4	1.35×10^5	0.9945
		HM	5.75×10^5	1.93×10^4	-1.87×10^2	5.30×10^4	1.55×10^5	0.9984
		Average	5.25×10^5	1.88×10^4	-1.77×10^2	4.80×10^4	1.45×10^5	

the loss of $11H_2 + 3/2O_2$ representing a weight loss of 24.84% and its calculated value is 26.70%. The final thermal products obtained at 800 °C are CoO + 12C.

3.6.5. $[Ni(cap)_2(H_2O)_2]\cdot 3H_2O$

The thermal degradation of the $[Ni(cap)_2(H_2O)_2]3H_2O$ complex take place in mainly one degradation stage. This stage occurs at a maximum temperature of 319 °C and accompanied by weight of loss 60.54% corresponding to the loss of five water molecules (coordinated and uncoordinated water molecules) and an organic part $C_6H_{22}O_3$ (organic moiety). Theoretically, the loss of these molecules corresponds to a weight loss of 61.27%.

3.6.6. $[Zn(cap)_2]$

As mentioned above in the nickel(II) complex, the zinc(II) caproate, $[Zn(cap)_2]$ complex, also has only one decomposition step. This step located in the range between 50 and 450 °C at maximum temperature $DTG_{max} = 310$ °C and the weight loss at this step is 72.65% due to the loss of $C_{12}H_{22}O_3$ organic moiety in agreement with the theoretical weight loss value of 72.37%. The final formed product at 800 °C is ZnO.

3.6.7. $[ZrO(cap)_2]\cdot 3H_2O$

The thermal decomposition of $[ZrO(cap)_2]\cdot 3H_2O$ complex proceeds with two main degradation steps. The first step of the degradation occurs at maximum temperature of 193 °C in the ranged of 30–250 °C is accompanied by the formation of anhydrous zirconyl(II) caproate complex with weight loss of 13.48% correspond to the loss of the three uncoordinated water molecules. Theoretically the loss of these molecules corresponds to a weight loss of 13.80% which agree with the experimental results. The second decomposition stage occurs at the maximum temperature 324 °C. The weight loss at this step is 40.59% associated with the loss of $C_7H_{22}O_3$ organic part. The theoretical weight loss value is 39.37%. The final residue at the end of this stage is ZrO_2.

3.6.8. $[UO_2(cap)(NO_3)]$

The degradation of the $[UO_2(cap)(NO_3)]$ complex take place in only one sharp decomposition step. The weight found for the residue after decomposition is 76.55% giving an actual total weight loss of 23.45% in agreement with our calculated total weight loss value of 23.48%. The degradation patterns of this complex are $NO_2 + 11/2H_2 + 3/2O_2$.

3.6.9. $[Zr(cap)_2(Cl)_2]$

The thermal decomposition data obtained support the proposed structure and indicate that, the thermal decomposition of this complex proceeds with two main degradation steps. The first stage of decomposition occurs at a temperature maximum of 174 °C. The found weight loss associated with this step is 15.50% and may be attributed to the loss of the organic moiety (C_4H_{10}) which is in good agreement with the calculated value of 14.79%. The second step of decomposition occurs at a temperature maximum of 346 °C. The weight loss found at this step equals to 38.95% corresponds to the loss of $C_3H_{12}O_2$ (organic moiety) and chlorine molecule. The theoretical value of weight loss of is 38.49%. The ZrO_2 is the final product formed at 800 °C.

3.6.10. $[Th(cap)_4]$

The $[Th(cap)_4]$ complex showed the absence of water molecules and the total weight loss was 63.13% with only one decomposition step. This step occurs in the range of 50–450 °C corresponds to a weight loss of molecular weight of 428 units ($C_{24}H_{44}O_6$; organic moiety), implied in a 1:4 (metal-to-ligand) complex in accordance with the analytical data. The theoretical value of weight loss is 61.85%. The ThO_2 is the final stable residue.

3.7. Kinetic studies

In recent years there has been increasing interest in determining the rate-dependent parameters of solid-state non-isothermal decomposition reactions by analysis of TG curves. Several equations [33–40] have been proposed as means of analyzing a TG curve and obtaining values for kinetic parameters. Many authors [33–37] have discussed the advantages of this method over the conventional isothermal method. The rate of a decomposition process can be described as the product of two separate functions of temperature and conversion [34], using

$$\frac{d\alpha}{dt} = k(T)f(\alpha) \tag{1}$$

where α is the fraction decomposed at time t, $k(T)$ is the temperature dependent function and $f(\alpha)$ is the conversion function dependent on the mechanism of decomposition. It has been established that the temperature dependent function $k(T)$ is of the Arrhenius type and can be considered as the rate constant k

$$k = A\,e^{-E^*/RT} \tag{2}$$

where R is the gas constant in (J mol^{-1} K^{-1}). Substituting equation (2) into equation (1), we get

$$\frac{d\alpha}{dT} = \left(\frac{A}{\varphi\,e^{-E^*/RT}}\right) f(\alpha)$$

Table 9
Antibacterial activity data of the caproic acid and their complexes

Compound	*Escherichia coli*	*Streptococcus penumonia*	*Bacillus subtilis*
Hacap	++++	++++	+++
$[Cr(cap)_3]\cdot 5H_2O$	−	++	−
$[Mn(cap)_2(H_2O)_2]$	−	−	−
$[Fe(cap)_3]\cdot 12H_2O$	++	−	−
$[Co(cap)_2(H_2O)_2]\cdot 4H_2O$	−	−	+++
$[Ni(cap)_2(H_2O)_2]\cdot 3H_2O$	−	−	−
$[Zn(cap)_2]$	++	++	−
$[ZrO(cap)_2]\cdot 3H_2O$	+++	+++	−
$[UO_2(cap)(NO_3)]$	+++	++	++
$[Zr(cap)_2(Cl)_2]$	+++	−	−
$[Th(cap)_4]$	++	−	++

−: NO antibacterial activity, +: mild activity, ++: moderate activity, +++: marked activity, ++++: strong marked activity.

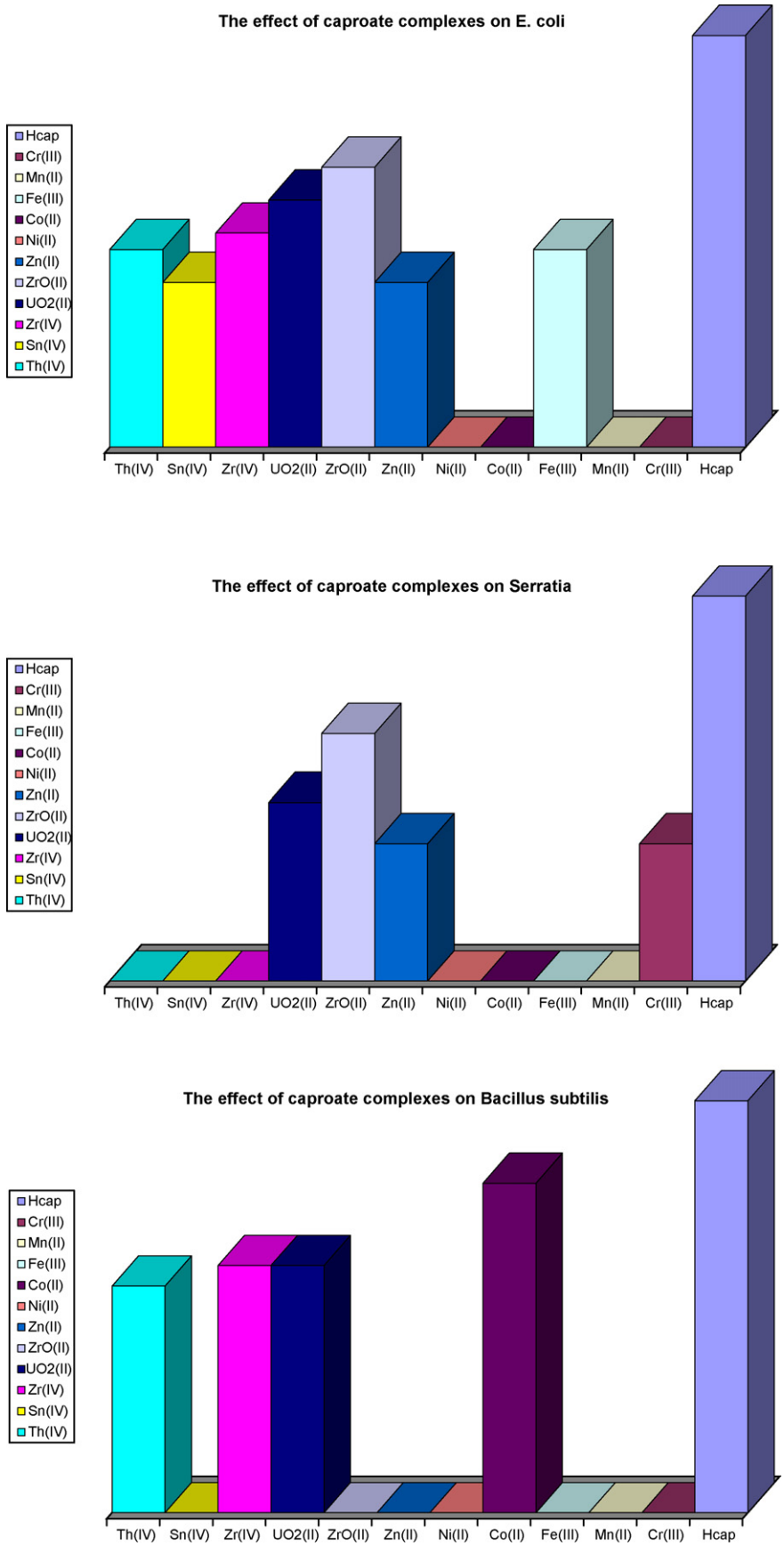

Fig. 5. The inhabitation zone of the caproic acid and its metal complexes on some kinds of bacterial.

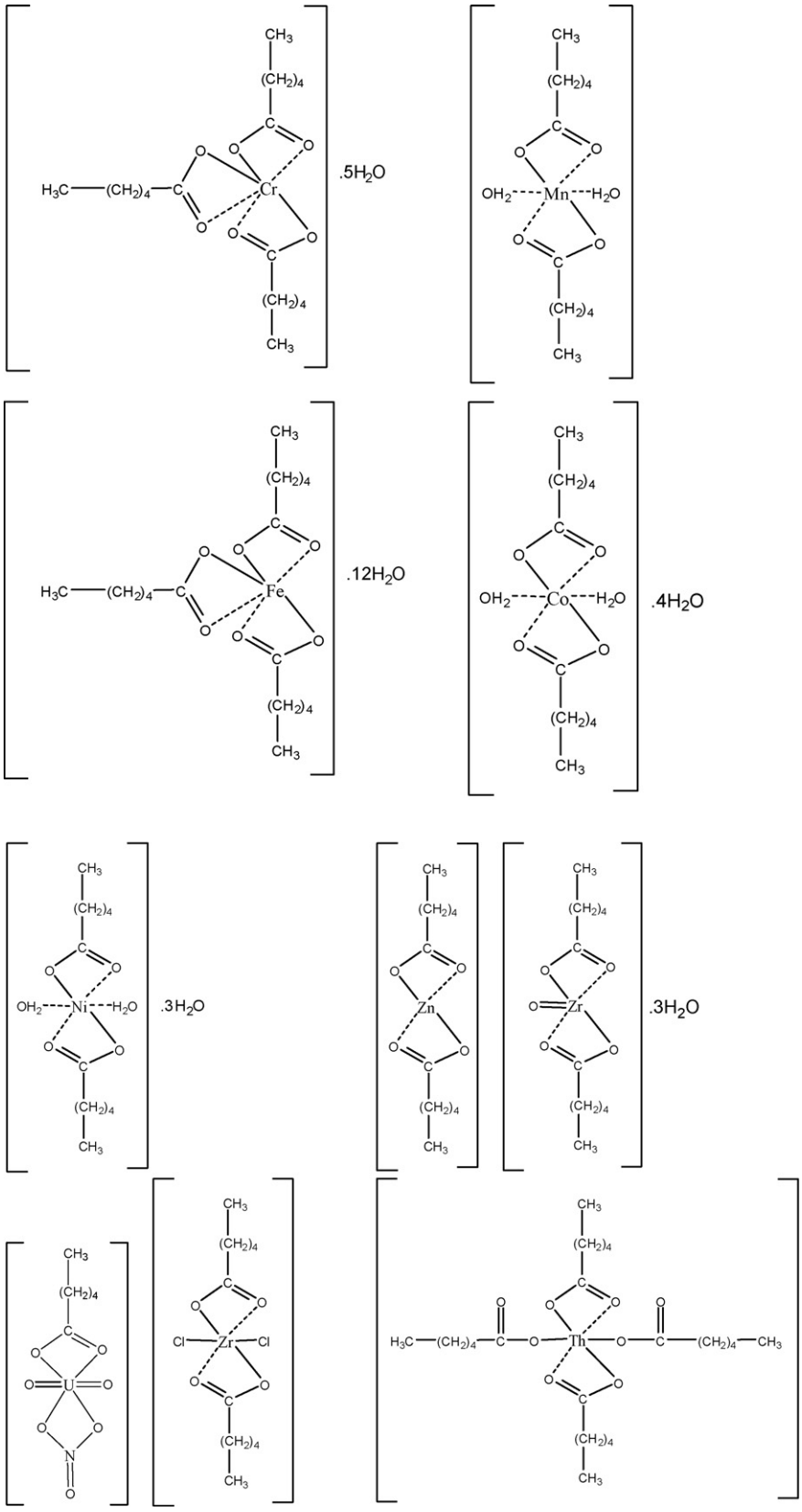

Scheme 3. The structures of caproate complexes.

where φ is the linear heating rate dT/dt. On integration and approximation, this equation can be obtained in the following form

$$\ln\ g(\alpha) = -\frac{E^*}{RT} + \ln\left[\frac{AR}{\varphi E^*}\right]$$

where $g(\alpha)$ is a function of α dependent on the mechanism of the reaction. The integral on the right hand side is known as temperature integral and has no closed for solution. So several techniques have been used for the evaluation of temperature integral. Most commonly used methods for this purpose are the differential method of Freeman and Carroll [33] integral method of Coat and Redfern [35], the approximation method of Horowitz and Metzger [38].

In the present investigation, the general thermal behaviors of the caproate complexes in terms of stability ranges, peak temperatures and values of kinetic parameters, are shown in Fig. 4 and Table 8. The kinetic parameters have been evaluated using the following methods and the results obtained by these methods are well agreement with each other. The following two methods are discussed in brief.

3.7.1. Coats–Redfern equation

The Coats–Redfern equation, which is a typical integral method, can be represented as:

$$\int_0^{\alpha} \frac{\mathrm{d}\alpha}{(1-\alpha)^n} = \frac{A}{\varphi}\int_{T_1}^{T_2} \exp\left(-\frac{E^*}{RT}\right)\mathrm{d}t$$

For convenience of integration the lower limit T_1 is usually taken as zero. This equation on integration gives

$$\ln\left[-\frac{\ln(1-\alpha)}{T^2}\right] = -\frac{E^*}{RT} + \ln\left[\frac{AR}{\varphi E^*}\right]$$

A plot of left-hand side (LHS) against $1/T$ was drawn. E^* is the energy of activation in J mol^{-1} and calculated from the slop and A in (s^{-1}) from the intercept value. The entropy of activation ΔS^* in (J K^{-1} mol^{-1}) was calculated by using the equation:

$$\Delta S^* = R\ \ln\left(\frac{Ah}{k_B\ T_s}\right) \tag{3}$$

where k_B is the Boltzmann constant, h is the Plank's constant and T_s is the DTG peak temperature [41].

3.7.2. Horowitz–Metzger equation

The Horowitz–Metzger equation is an illustrative of the approximation methods. These authors derived the relation:

$$\log\left[\frac{\{1-(1-\alpha)^{1-n}\}}{(1-n)}\right] = \frac{E^*\theta}{2.303RT_s^2} \quad \text{for } n \neq 1 \tag{4}$$

when $n = 1$, the LHS of equation (4) would be $\log[-\log(1-\alpha)]$. For a first-order kinetic process the Horowitz-Metzger equation may be written in the form:

$$\log\left[\log\left(\frac{w_\alpha}{w_\gamma}\right)\right] = \frac{E^*\theta}{2.303RT_s^2} - \log\ 2.303$$

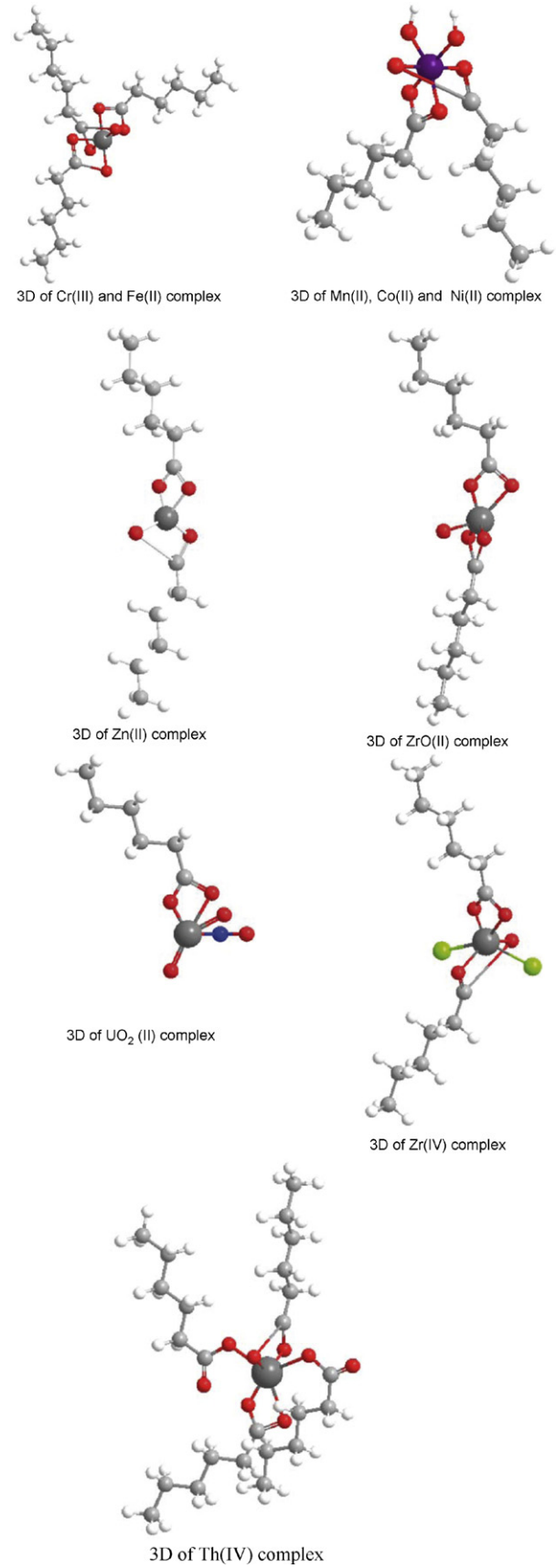

Scheme 4. The three dimensional of caproate complexes.

where $\theta = T - T_s$, $w_\gamma = w_\alpha - w$, w_α = mass loss at the completion of the reaction; w = mass loss up to time t. The plot of $\log[\log(w_\alpha/w_\gamma)]$ versus θ was drawn and found to be linear from the slope of which E^* was calculated. The pre-exponential factor, A, was calculated from the equation:

$$\frac{E^*}{RT_s^2} = \frac{A}{[\varphi \exp(-E^*/RT_s)]}$$

The entropy of activation, ΔS^*, was calculated from equation (3). The enthalpy activation, ΔH^*, and Gibbs free energy, ΔG^*, were calculated from; $\Delta H^* = E^* - RT$ and $\Delta G^* = \Delta H^* - T\Delta S^*$, respectively.

3.8. Antibacterial investigation

The results of antibacterial activities in vitro of the ligand and the complexes are shown in Table 9 and Fig. 5. The minimal inhibitory concentration values listed in Table 9 show that all the test complexes have been obstructed the activity of caproic acid against the order of antibacterial.

3.9. Structure of the caproate complexes

Accordingly, the above-mentioned discussions using elemental analysis, magnetic studies, molar conductance, (infrared and ^{1}H NMR) spectra as well as thermogravimetric analysis; the suggested structures of the caproate complexes can be represented in Schemes 3 and 4.

References

[1] R.C. Mehrotra, R. Bohra, Metal Carboxylates, Academic Press, London, 1983.
[2] B.P. Baranwal, S.S. Das, P. Singh, Synth. React. Inorg. Met. Org. Chem. 28 (1998) 1689.
[3] E.J. Baran, S.B. Etcheverry, M.H. Torre, E. Kremer, Polyhedron 13 (12) (1994) 1859.
[4] G.C. Campbell, J.F. Haw, Inorg. Chem. 27 (1988) 3706.
[5] G.C. Campbell, J.H. Reibenspies, J.F. Haw, Inorg. Chem. 30 (1991) 171.
[6] R.D. Harcourt, F.L. Skrezenek, R.G.A.R. Maclagan, J. Am. Chem. Soc. 108 (1986) 5403.
[7] R.D. Harcout, G.E. Martin, J. Chem. Soc. Faraday Trans. II 73 (1977) 114.
[8] M. Kato, Y. Muto, Coord. Chem. Rev. 92 (1988) 45.
[9] F.P.W. Agterberg, H.A.J. Provó Kluit, W.L. Driessen, H. Oevering, W. Buijs, M.T. Lakin, A.L. Spek, J. Reedijk, Inorg. Chem. 36 (1997) 4321.
[10] A. Zell, H. Einspahr, C.E. Bugg, Biochemistry 24 (1985) 533.
[11] V.L. Pecoraro, M.J. Baldwin, A. Gelasco, Chem. Rev. 94 (1994) 807.
[12] E.V. Brusau, J.C. Pedregosa, G.E. Narda, E.P. Ayala, E.A. Oliveira, J. Arg. Chem. Soc. 92 (1/3) (2004) 43.
[13] S. Budavari (Ed.), The Merck Index Text Book, 12th ed., Rahway, NJ, 1998, p. 286.
[14] F. Beilstein, Handbuch der Organischem Chemie, Bd. IX, Springer Verlag, Berlin, 1926.
[15] L.L. Kolomiets, O.V. Lysenko, I.V. Pyatnitskii, Z. Anal. Khim. 43 (10) (1988) 1773.
[16] I.V. Pyatnitskii, L.L. Kolomeits, O.V. Lysenko, M.G. Sobko, Z. Anal. Khim. 45 (1) (1990) 56.
[17] S. Kopacz, J. Szantula, T. Pardela, Z. Prikladoni Khim. 62 (11) (1989) 2535.
[18] R. Pietsch, Anal. Chim. Acta 53 (2) (1971) 287.
[19] T.N. Gushchina, G.A. Kotenko, Koord. Khim. 12 (3) (1986) 325.
[20] W. Brzyska, B. Paszkowska, J. Therm. Anal. 51 (1998) 561.
[21] A. Doyle, J. Felcman, M. Gambardella, C.N. Verani, M.L.B. Tristao, Polyhedron 19 (26/27) (2000) 2621.
[22] M.S. Refat, D.N. Kumar, R.F. De Farias, J. Coord. Chem. 59 (16) (2006) 1857.
[23] K. Burger, Coordination Chemistry: Experimental Methods, Butterworth Group, Britain, 1973.
[24] M.S. Refat, J. Mol. Struct., in press.
[25] M.A. Mesubi, J. Mol. Struct. 81 (1982) 61.
[26] K. Nakamato, P.J. Mc Carthy, Spectroscopy and Structure of Metal Chelate Compounds, John Wiley, New York, 1968, p. 268.
[27] R. Goto, T. Takenaka, J. Chem. Soc. Jpn. 84 (1963) 392.
[28] L.S. Gelfand, F.J. Iaconianni, L.L. Pytlewski, A.N. Speca, C.M. Mikulski, N.M. Karayannis, J. Inorg. Nucl. Chem. 42 (1980) 377.
[29] A. Earnshow, Introduction to Magneto Chemistry, Academic Press, New York, 1968.
[30] G.D. Fasman, Handbook of Biochemistry and Molecular Biology, Nucleic acids, vol. I, CRC Press, pp. 65–215.
[31] R.H. Holm, F.A. Cotton, J. Am. Chem. Soc. 80 (1958) 5658.
[32] F.A. Cotton, C.W. Wilkinson, Advanced Inorganic Chemistry, 3rd ed., Interscience Publisher, New York, 1972.
[33] E.S. Freeman, B. Carroll, J. Phys. Chem. 62 (1958) 394.
[34] J. Sestak, V. Satava, W.W. Wendlandt, Thermochim. Acta 7 (1973) 333.
[35] A.W. Coats, J.P. Redfern, Nature 201 (1964) 68.
[36] T. Ozawa, Bull. Chem. Sot. Jpn. 38 (1965) 1881.
[37] W.W. Wendlandt, Thermal Methods of Analysis, Wiley, New York, 1974.
[38] H.W. Horowitz, G. Metzger, Anal. Chem. 35 (1963) 1464.
[39] J.H. Flynn, L.A. Wall, Polym. Lett. 4 (1966) 323.
[40] P. Kofstad, Nature 179 (1957) 1362.
[41] J.H.F. Flynn, L.A. Wall, J. Res. Natl. Bur. Stand. A 70 (1996) 487.